Journal of Applied Fluid Mechanics, Vol. 16, No. 3, pp. 519-531, 2023.
Available online at www.jafmonline.net, ISSN 1735-3572, EISSN 1735-3645.
https://doi.org/10.47176/jafm.16.03.1342

Influence of Inlet Vane and Wrap Angles on Cavitation Behavior of a Centrifugal Pump

A. H. Dönmez[1†], Z. Yumurtacı[2] and L. Kavurmacıoğlu[3]

[1] *Halic University, Istanbul, 34060, Turkey*
[2] *Yildiz Technical University, Istanbul, 34349, Turkey*
[3] *Istanbul Technical University, Istanbul, 34437, Turkey*

†*Corresponding Author Email: aydindonmez@halic.edu.tr*

(Received May 26, 2022; accepted October 11, 2022)

ABSTRACT

This comprehensive study focuses on the relationship between the inlet vane and wrap angles of a centrifugal pump impeller and its cavitation behavior. The objective is to propose a new design for cavitation performance enhancement of the pump by reducing the required net positive suction head ($NPSH_R$). To render a detailed study, the variations of the mentioned angles were examined both at hub and shroud. A three-dimensional two-phase parametric computational fluid dynamics (CFD) study was conducted and variations of inlet blade and wrap angles at hub and shroud were investigated separately. After validating the experimental results with the pump model, the pump parameterization process was carried out, and pump geometry was re-defined with its geometrical properties. The characteristic curves of the parameterized pump and pump model were in agreement with each other. Numerical cavitation tests were performed and the NPSHR values of each design were calculated for four different operating conditions. Results showed that cavitation performance increase was achieved with angle variations at the best efficiency point (BEP) but, this situation led the pump to operate exposed to cavitation at high flows (HF) for some designs. Therefore, the design with the best cavitation performance increased at BEP and HF was proposed as a new design. During numerical simulations, shear stress transport (SST) turbulence model and Rayleigh–Plesset equation were used.

Keywords: Centrifugal pump; Cavitation; Inlet vane angle; Wrap angle; Two-phase flow; CFD.

NOMENCLATURE

H	pump head	α	volume fraction
k	turbulence kinetic energy	β	blade angle
n_q	specific speed	θ	wrap angle
P	pressure	μ	molecular dynamic viscosity
Q	volumetric flow rate	μ_t	turbulent viscosity
R_b	bubble radius	γ	eddy viscosity
S	invariant measure of the strain rate	ρ	fluid density
u	velocity	σ	surface tension
y	interval to the closest wall	ω	specific dissipation rate,
y^+	dimensionless wall distance		

1. INTRODUCTION

Avoiding cavitation is crucial during the operation of centrifugal pumps. The cavitation performance of a pump is highly affected by the impeller inlet geometry (Luo *et al*. 2008; Bonaiuti *et al.* 2010). Also, as the vane tip shape becomes rounder and thinner, the cavitation performance of the pump increases (Yokoyama 1960; Christopher and Kumaraswamy 2013). Furthermore, inlet vane angle (Vujanic and Velensek 1994; Friedrichs and Kosyna 2002; Gaetani *et al*. 2012; Pei *et al*. 2017) and wrap angle (Weidong *et al*. 2009; Bing and Cao 2013; Tan *et al*. 2014a; Pei *et al*. 2017) are important parameters that determine the performance of a centrifugal pump.

There are several numerical pump simulation studies validated with experiments in the literature. Li *et al*. (2013) conducted experimental and numerical studies to observe the cavitation in a centrifugal

pump and showed the relationship between cavitation and head drop. Lu *et al.* (2017) conducted experimental studies to obtain pressure fluctuations, vibration characteristics, and internal flow instabilities at the inlet and outlet of a centrifugal pump. The relationship between vibration and cavitation development was also investigated. Tan *et al.* (2014b) performed experimental and numerical studies to examine the fluid flow characteristics of a centrifugal pump at partial load (0.76 Q) and high flow (1.2 Q) conditions. Observations indicated that the cavitation occurrence had much more effect on flow pattern at partial load conditions. Liu *et al.* (2013) investigated the sheet cavitation of a centrifugal pump blade both experimentally and numerically. Accordingly, a filter-based k – ε turbulence model was used considering the anisotropic effect of the swirl characteristic. Sheet cavities were observed at the suction side of the vanes. Coutier-Delgosha *et al.* (2003) conducted numerical studies on a centrifugal pump with a specific speed of 20 $\left(n_q = \frac{n\sqrt{Q}}{H^{3/4}}\right)$ and developed a new model for three-dimensional cavitating flows to estimate the cavitation characteristics of turbomachinery. The formation and growth of cavities were observed as the inlet pressure was decreased using flow visualizations. Shao *et al.* (2018) observed the gas and liquid flow patterns in a centrifugal pump with high-speed photography. Findings indicated that the initial liquid volume flow rate had a critical effect on the critical gas volume flow rate, rather than the rotational speed. Valentini *et al.* (2017) conducted experiments to characterize the rotodynamic forces on an unshrouded impeller of a centrifugal pump under varying flow rates and cavitation conditions. A newly developed method was used t**o** measure the forces with different cavitation numbers at a fixed whirl ratio value. Ye *et al.* (2017), proposed a semi-analytical model to observe the cavitation in centrifugal pumps. For this purpose, experimental results at different flow rates were compared with both their semi-analytical and Zwart methods, and head, cavity length water vapor volume fractions of the experimental and numerical studies were compared.

Optimization and geometrical modifications of the pumps were investigated for increasing their performance. Zhang *et al.* (2019) performed experimental and numerical studies for investigating the effect of trailing edge profile on unsteady pressure pulsations. Accordingly, over a 20% decrease in pressure amplitude measurements was achieved with the new proposed profile. Shim *et al.* (2018) conducted an optimization on a centrifugal pump impeller to reduce the recirculation at the inlet and decrease the cavitation at off-design conditions. Using a genetic algorithm, six different Pareto designs were proposed, and a significant improvement of specified objective functions was achieved concerning the reference design. Mousmoulis *et al.* (2019) studied cavitation formation and growth on three impellers with different vane profiles. For this purpose, vibration and acoustic measurements were conducted with flow visualization. Kang *et al.* (2017) mentioned that the cavitation performance of the centrifugal pumps was directly related to the geometric properties of their vane and compared three different impeller designs of a cavitating centrifugal pump. According to the numerical simulations the hydraulic performances of the impellers were similar; however, cavitation performances were different from each other. Luo *et al.* (2013) conducted numerical studies to figure out the cavitating flow in a centrifugal pump with two different approaches and found out that decreasing cavitation number resulted in a performance loss of the pump. Xu *et al.* (2016) carried out a multi-objective study on a centrifugal pump and compared 16 impellers derived from five different parameters. They succeeded to obtain a design with both a 3.09 % hydraulic and 1.45 m cavitation performance increase using the Taguchi method. Dönmez *et al.* (2019) investigated the cavitation performance of a centrifugal pump with varying inlet blade angles. They mentioned that inlet blade angle values could be different at hub and shroud so, the effect of hub and shroud inlet blade angles were examined separately. Pump characteristic curves and cavitation tests were conducted numerically, and design comparisons were made using water vapor mass fractions.

Inlet vane and wrap angles may have different values at the hub and shroud of the impeller due to their unique designs. This situation requires investigating the effect of those angles both at hub and shroud surfaces. In the literature, this kind of approach is limited.

This study is significant because while the variation of inlet vane and wrap angles has a limited effect on pump efficiency, they have a remarkable influence on the cavitation performance of the pump. Furthermore, the effect of inlet vane and wrap angles on the cavitation behavior of an existing centrifugal pump was investigated both at hub and shroud, respectively. From this point of view, this study is unique and novel. For this purpose, we conducted a numerical study on a commercial centrifugal pump model and the results were compared with the experimental data. Afterwards, the pump impeller was parameterized by means of inlet and outlet vane angles, wrap angle, vane thickness, and other geometrical aspects. According to the numerical study conducted on the parameterized impeller, the results were in agreement with the previous numerical study. A two-phase 3D numerical study was performed on the parameterized pump and the effect of inlet vane and wrap angles were investigated, respectively. Since the aforementioned angles had different values at hub and shroud, the effect of those angles was investigated separately. Variations of the mentioned angles had different impacts on the off-design and on-design conditions so, the results were tabulated and presented for four different flow rate conditions.

2. NUMERICAL SIMULATION OF THE PUMP

The study started with a numerical simulation of the existing impeller. Experimental results and CAD

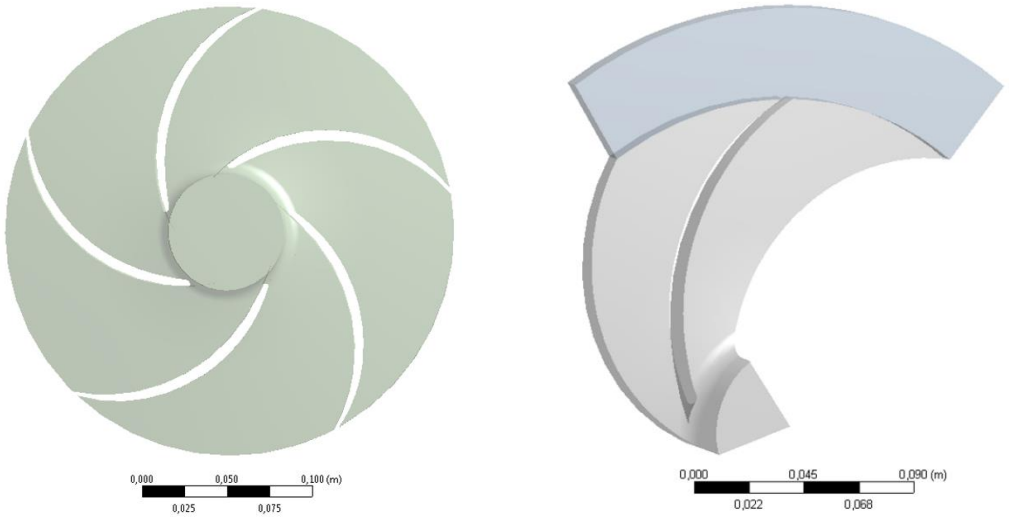

(a) (b)

Fig. 1. Flow volume of the impeller. a) whole impeller, b) single passage with vaneless diffuser

drawings of the impeller were procured from the manufacturer company of the pump. The impeller had five vanes so, the flow volume was cut with the help of the ANSYS SpaceClaim module and one-fifth of the impeller was considered for the meshing procedure. The single passage solution aimed to minimize the computational time requirement with rotational periodic boundary conditions. Afterward, the outlet domain was extended to represent the vaneless diffuser. The properties of the pump at on-design conditions are illustrated in Table 1. and the computational domain is presented in Fig. 1.

2.1 Turbulence Modeling

Shear Stress Transport (SST) k-ω turbulence model was used in this study, which was a widely used model in turbomachinery CFD simulations due to its noticeable advantages as a combination of k-ε and k-ω turbulence models. SST turbulence model employs the k-ε turbulence model in the free stream and switches to the k-ω model in the boundary layer, which enables faster and more accurate computation. Governing equations of the turbulence model starting from turbulence kinetic energy (k) and specific dissipation rate (ω) are presented below (Menter 1994).

Table 1. Technical properties of the pump.

Specification	Value
Head [m]	90.55
Discharge [m^3/h]	59.9
Specific speed	13
Number of vanes	5
Impeller diameter [mm]	264
Efficiency [%]	61
$NPSH_R$ [m]	5.36

$$\frac{\partial(\rho k)}{\partial t}+\frac{\partial(\rho U_i k)}{\partial x_i}=\tilde{P}_k-\beta^*\rho k\omega+\frac{\partial}{\partial x_i}\left[(\mu+\sigma_k\mu_t)\frac{\partial k}{\partial x_i}\right] \tag{1}$$

$$\frac{\partial(\rho\omega)}{\partial t}+\frac{\partial(\rho U_i k)}{\partial x_i}=\alpha\rho S^2-\beta\rho\omega^2+\frac{\partial}{\partial x_i}\left[(\mu+\sigma_\omega\mu_t)\frac{\partial\omega}{\partial x_i}\right] +2(1-F_1)\rho\sigma_{\omega 2}\frac{1}{\omega}\frac{\partial k}{\partial x_i}\frac{\partial\omega}{\partial x_i} \tag{2}$$

The definitions of the parameters are as follows:

$$F_1=\tanh\left\{\left\{\min\left[\max\left(\frac{k^{1/2}}{\beta^*\omega y},\frac{500\nu}{y^2\omega}\right),\frac{4\rho\sigma_{\omega 2}k}{CD_{k\omega}y^2}\right]\right\}^4\right\} \tag{3}$$

$$CD_{k\omega}=\max\left(2\rho\sigma_{\omega 2}\frac{1}{\omega}\frac{\partial k}{\partial x_i}\frac{\partial\omega}{\partial x_i},10^{-10}\right) \tag{4}$$

$$\nu_t=\frac{a_1 k}{\max(a_1\omega,SF_2)} \tag{5}$$

$$F_2=\tanh\left[\left[\max\left(\frac{2k^{1/2}}{\beta^*\omega y},\frac{500\nu}{y^2\omega}\right)\right]^2\right] \tag{6}$$

$$P_k=\mu_t\frac{\partial U_i}{\partial x_j}\left(\frac{\partial U_i}{\partial x_j}+\frac{\partial U_j}{\partial x_i}\right)\rightarrow\tilde{P}_k=\min(P_k,10\cdot\beta^*\rho k\omega) \tag{7}$$

In the equations above, S represents the invariant measure of the strain rate. F_1 and F_2 are blending functions. ρ is the fluid density, ν_t is turbulent kinematic viscosity and defined as μ_t/ρ. μ is molecular dynamic viscosity and y is the interval to the closest wall. The values of the constants in the equations are presented below.

$\alpha_1 = 5/9$, $\alpha_2 = 0.44$, $\beta_1 = 3/40$, $\beta_2 = 0.0828$, $\beta^* = 0.09$, $\sigma_{k1} = 0.85$, $\sigma_{k2} = 1$, $\sigma_{\omega 1} = 0.5$, $\sigma_{\omega 2} = 0.856$

2.2 Cavitation Modeling

Due to the two-phase modeling, the selection of a cavitation model is essential. Water at 25 °C and water vapor at 25 °C were selected as working fluids to observe the vaporization regions in the computational domain. At 25 °C, the water vapor pressure was specified as 3169 Pa.

The Rayleigh-Plesset equation describes bubble behavior in flow and assumes that cavitation occurs by the formation of nuclei, bubble growth, and collapse. The cavitation bubbles were assumed spherical. Governing equation of the cavitation model is presented below (Brennen 1995).

$$\frac{p_B(t)-p_\infty(t)}{\rho_l}=R_b\frac{\partial^2 R_b}{\partial t^2}+\frac{3}{2}\left(\frac{\partial R_b}{\partial t}\right)^2+\frac{4\nu_L}{R_b}\frac{dR_b}{dt}+\frac{2\sigma}{\rho_L R_b} \tag{8}$$

In the equation, p_B and p_∞ are bubble surface pressure and ambient pressure, respectively. ρ_l is liquid density ν_L is liquid kinematic viscosity, R_b is the radius of spherical cavitation bubble and σ is surface tension. Zwart-Gerber-Belamri cavitation model was implemented during whole simulations.

2.3 Boundary Conditions

In this section, the pump characteristic curve was obtained numerically to compare with the experimental results. Accordingly, variation of the pump head was calculated for different flow rates. For this purpose, the mass flow boundary condition was set at the outlet, and the changes at the pump head were obtained with the varying discharge. At the inlet, the total pressure boundary condition was used. Solid surfaces like hub, shroud, and vane were defined as walls. The rotational periodic boundary condition was defined to the sides of the computational domain.

2.4 Mesh Generation on Impeller Model

SST turbulence model was used in this study. Therefore, near-wall treatment was applied at the hub, shroud, and vane surfaces to keep the dimensionless wall distance (y^+) value under 3 and capture the gradients in detail. Tetrahedrons in the single passage flow volume and hexahedrons on the vaneless diffuser were adopted using Ansys Meshing. Details of the adopted grid can be seen in Fig. 2.

2.5 Mesh Independency Study on Impeller Model

Mesh independence is a crucial study to be carried out in any kind of CFD simulation because the results can vary with the grid size. As the grid size decrease, any physical parameter in the computational domain, e.g., head, will converge to a constant value. On the other hand, computational requirements and time will increase. So, a grid-independent solution with minimum computational cost must be achieved. To conduct the simulations, three different mesh schemes were adopted in the computational domain. The total number of elements for mentioned schemes and calculated pump head values are presented in Fig. 3.

According to the figure, there is a 5% increase in the head as the meshing scheme changes from coarse to medium. However, even though the total number of elements doubles, there is no significant change in the head when the mesh scheme is changed from

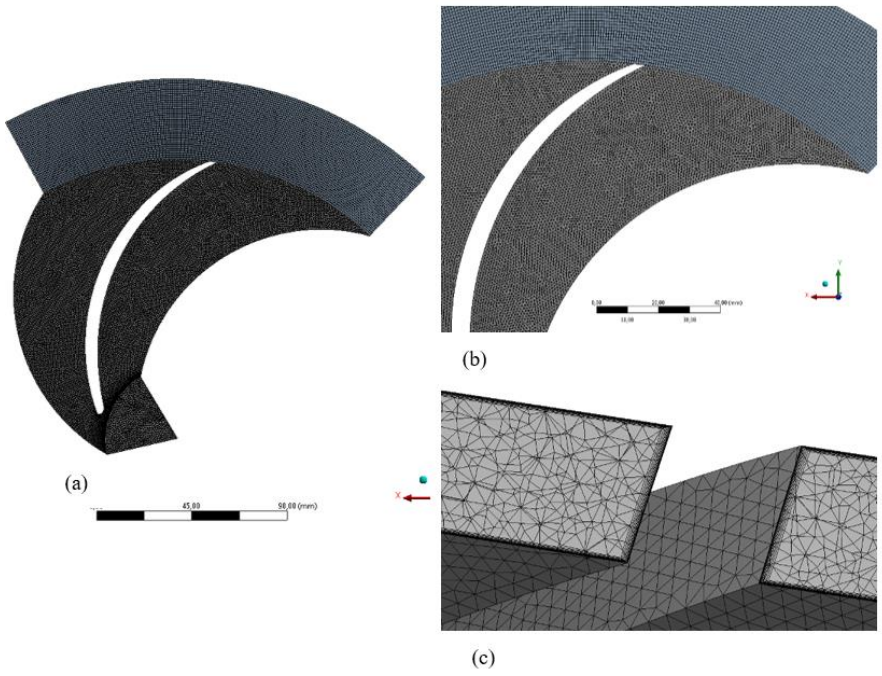

Fig. 2. Mesh generation on computational domain a) single passage b) tetrahedrons on impeller and hexahedrons on vaneless diffuser c) boundary layer mesh on the wall.

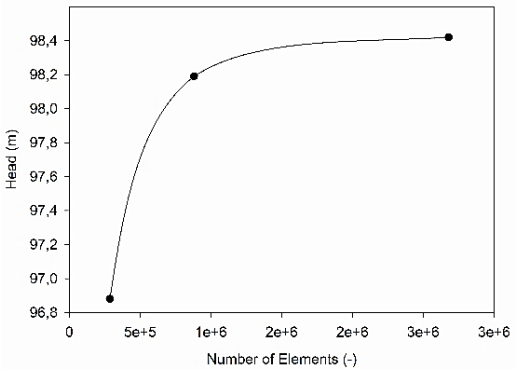

Fig. 3. Mesh independency study of solid model.

medium to fine. So, the medium mesh scheme with 880,468 elements is chosen according to the mesh independence study.

2.6 CFD Studies

Numerical simulation is performed by iterative simultaneous solution of Navier-Stokes and continuity equations under the homogenous fluid assumption using Ansys CFX. Governing equations of the models are solved with the finite volume method. All discretization operations are implemented as second-order accurate in space based on a Taylor series expansion.

The fluid consists of liquid water and water vapor; therefore, continuity and momentum equations contain mixture terms and are presented in the equations below. The fluid consists of liquid water and water vapor therefore, continuity and momentum equations contain mixture terms and are presented in the equations below.

$$\frac{\partial \rho_m}{\partial t} + \frac{\partial (\rho_m u_i)}{\partial x_i} \tag{9}$$

$$\frac{\partial (\rho_m u_i)}{\partial t} + \frac{\partial (\rho_m u_i u_j)}{\partial x_j} = -\frac{\partial p}{\partial x_i} + \frac{\partial}{\partial x_i}\left[(\mu_m + \mu_t)\left(\frac{\partial u_i}{\partial x_j} + \frac{\partial u_j}{\partial x_i} - \frac{2}{3}\frac{\partial u_k}{\partial x_k}\delta_{ij} \right) \right] \tag{10}$$

where,

$$\rho_m = \rho_l \alpha_l + \rho_v \alpha_v \tag{11}$$

$$\mu_m = \mu_l \alpha_l + \mu_v \alpha_v \tag{12}$$

Here, u is velocity, and α is the volume fraction of the fluids. Subscripts i, j, and k represent directions in Cartesian coordinates, and l, v, and m stand for liquid, vapor, and mixture phases, respectively. Furthermore, the y^+ distribution along the suction and pressure sides of the vane can be seen in Fig. 4.

Figure 4 shows the y^+ variation on suction and pressure surfaces of the vane. Accordingly, the y^+ distribution along the vane provides the turbulence model requirement.

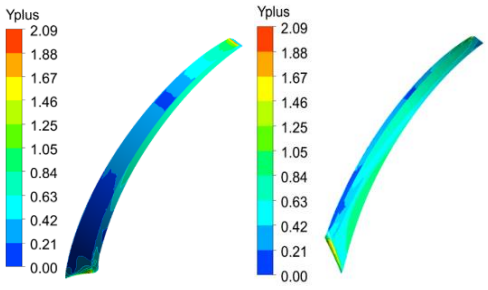

(a) (b)

Fig. 4. y^+ distribution along the vane

Thereafter, CFD simulations are carried out for different flow rates to obtain the pump characteristic curve numerically. The pump head is calculated via the difference between the outlet and inlet total pressures at the stationary frame divided by specific weight. The formula is presented in Equation 13.

$$H = \frac{P_{total\_outlet} - P_{total\_inlet}}{\rho g} \tag{13}$$

2.7 Experimental Study and Comparison of Experimental and Numerical Results

The experimental setup mainly consists of pressure transducers located at the inlet and outlet of the pump, a flow meter, a gate valve, and suction and discharge pipes. Firstly, the pump head-discharge characteristics curve is obtained by measuring the inlet and outlet pressures of the pump for varying flow rates. The flow rate adjustment is done by gate valve and pump head values are calculated from the pressure data. Afterwards, pump cavitation test is conducted by decreasing the inlet pressure step by step at a constant flow rate. This process is repeated at different flow rates and the pump $NPSH_R$-discharge curve is derived. The details of the experimental setup can be seen in Fig. 5.

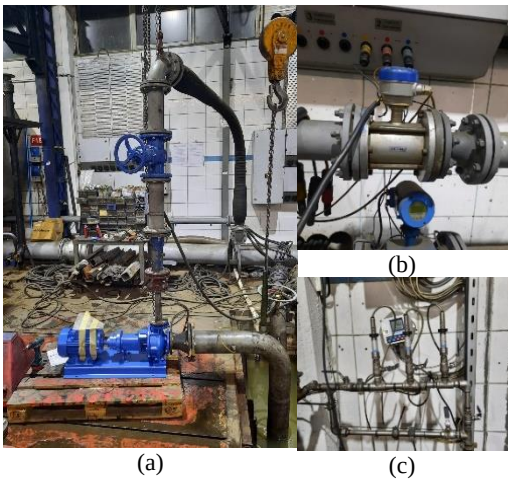

(a) (b) (c)

Fig. 5. Experimental setup a) pump, gate valve, and pipes b) flow meter c) pressure transducers.

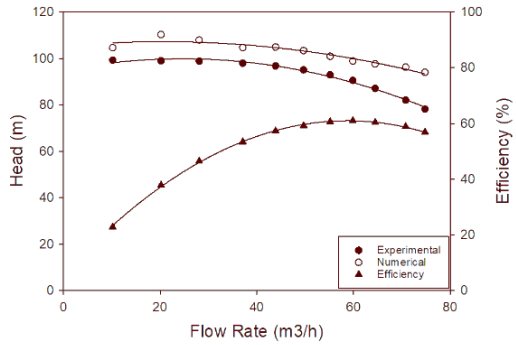

Fig. 6. Experimental and numerical pump characteristic curves.

The experimental and numerical pump characteristics curves can be seen in Fig. 6. Furthermore, pump efficiency curve is also presented. Hereunder, experimental, and numerical results are in good agreement with each other except at high flows (HF). The term HF describes the flow rate values above 125% of the flow rate at BEP.

It is obvious that there are experimental measurement errors. Furthermore, there are assumptions in the cavitation models during the numerical study. These issues may lead to a reasonable difference between the experimental and numerical pump characteristics curves.

3. PUMP PARAMETERIZATION

To achieve a parametric study, the pump impeller is defined by means of its geometrical features such as inlet and outlet vane angles, wrap angle, and vane thickness. From 20° to 50°, the inlet vane angle at the hub and shroud is increased by 10° at a time. A similar approach is implemented for the wrap angle. While the wrap angle at hub varies from 91° to 111°, the wrap angle at shroud deviates from 71° to 91° with 10° steps. The parameterization procedure is conducted using Ansys 16.0 BladeGen module. This is vital because the BladeGen module enables to carry out a parametric study by defining the aforementioned geometrical properties directly. This is useful to understand the effect of all parameters on the cavitation performance of the pump separately. Dimensional properties of the pump are measured from the CAD model directly and these values are set as input for the parameterized pump. The values of the measured impeller properties can be seen in Table 2.

Table 2. Impeller properties of the parameterized pump.

Impeller property	Value
Inlet vane angle at shroud ($\beta_{1shroud}$)	39°
Inlet vane angle at hub (β_{1hub})	32°
Outlet vane angle (β_2)	33°
Wrap angle at shroud (θ_{shroud})	81°
Wrap angle at hub (θ_{hub})	101°
Vane thickness	4 mm

The values of vane and wrap angles can be different at the hub and shroud surface of the impeller, especially due to the twisted structure of the vane. Thus, the values of the inlet vane and wrap angles of the examined pump are different at hub and shroud. Hereby, the effect of inlet vane and wrap angles are investigated both at hub and shroud in detail. While considering the wrap angle variation, a linear profile assumption is considered along the vane in streamwise direction (from leading edge to trailing edge).

3.1 Mesh Generation on Parameterized Pump

Since the impeller geometry is constituted by the BladeGen module, a mesh generation study is carried out with the Ansys TurboGrid module. TurboGrid is a useful tool to execute a boundary layer grid. Also, it is possible to adopt a structured grid within the whole flow passage. The details of the mesh on the parameterized pump are presented in Fig. 7.

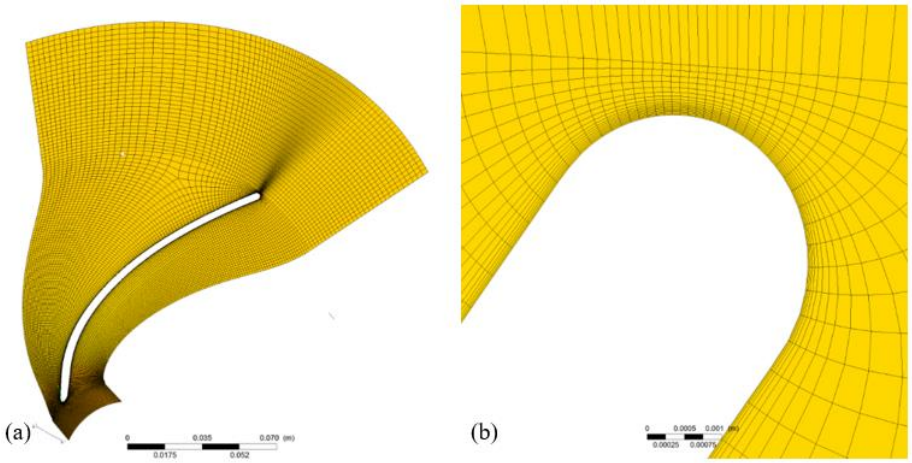

Fig. 7. Mesh generation on the parameterized pump a) single passage, b) boundary layer.

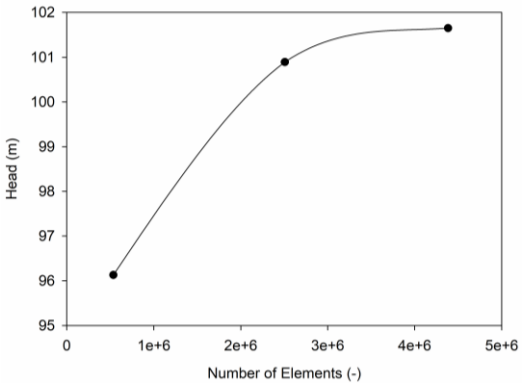

Fig. 8. Mesh independency study of parameterized pump.

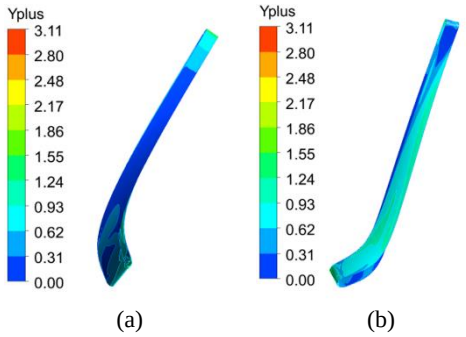

Fig. 9. y^+ distribution on parameterized pump's vane a) pressure side, b) suction side.

3.2 Mesh Independency Study on Parameterized Pump

Similar to the grid independence work in the previous section, a new mesh independence study is conducted in order to achieve a correct and fast computation. According to three different schemes; coarse, medium, and fine; variation of the pump head is calculated. Results are introduced in Fig. 8.

As it is seen, when the meshing scheme is changed from coarse to medium total pump head is increased by more than one meter. However, there is no significant head rise when the meshing scheme changed from medium to fine even though the total number of elements triples. For this reason, a medium-mesh scheme with 2,506,048 elements is selected to conduct CFD studies. Minimum orthogonal quality of the mesh is 0.133.

3.3 CFD Studies and Comparison of Parameterized Pump with Pump Model

SST k-ω turbulence model was used as the turbulence model within the whole study. y^+ distribution along the vane of the parameterized pump is presented in Fig.9.

The y^+ values exceeding 3 was only observed at the tip of the impeller as a point. Additionally, the mass flow average of y^+ values were 0.541 at the vane, 0.456 at the hub, and 0.477 at the shroud.

A similar study in the previous section was performed. To obtain the pump performance results of the parameterized pump, two-phase CFD simulations were conducted for varying flow rates. The same flow rate values in the previous numerical study were applied during simulations. As a result, the characteristic curve of the parameterized pump is obtained by using the same calculation methodology. The results of the two numerical characteristic curves are presented in Fig. 10.

The numerical pump characteristics of the pump model and parameterized pump were in good agreement. The slope of the parameterized pump is less than the pump model and at BEP the head values are overlapping and two numerical curves are intersecting. Figure 11 represents the relative error concerning the first numerical results.

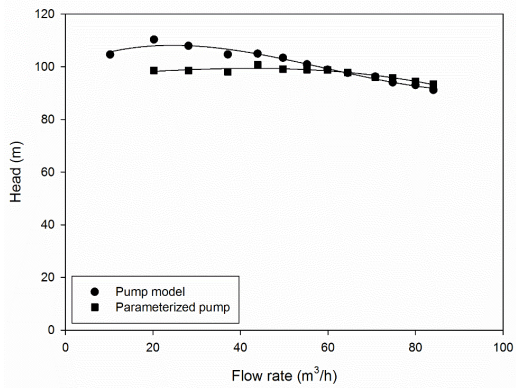

Fig. 10. Characteristic curves of the parameterized pump and pump model.

According to the figure, all data are between 10% error bands except at one flow rate value. This situation shows that the parameterized pump correctly represents the first pump model obtained from the manufacturer company. From now on, a parametric study can be conducted to investigate the effect of inlet vane and wrap angles both at hub and shroud to observe how the cavitation performance of the pump is affected by angle variations.

Accordingly, a numerical cavitation test is performed for different flow rate values. This is achieved by decreasing the inlet pressure step by step. Head drop occurrence is observed in all flow rates at different

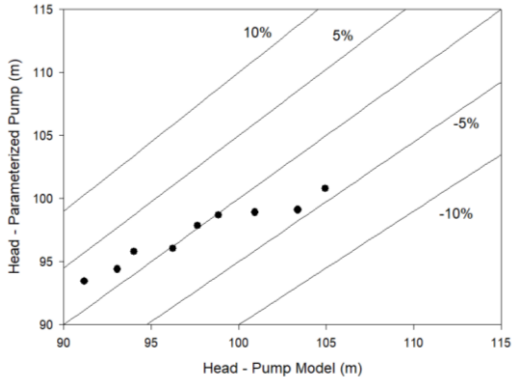

Fig. 11. Comparison of two numerical pump characteristics.

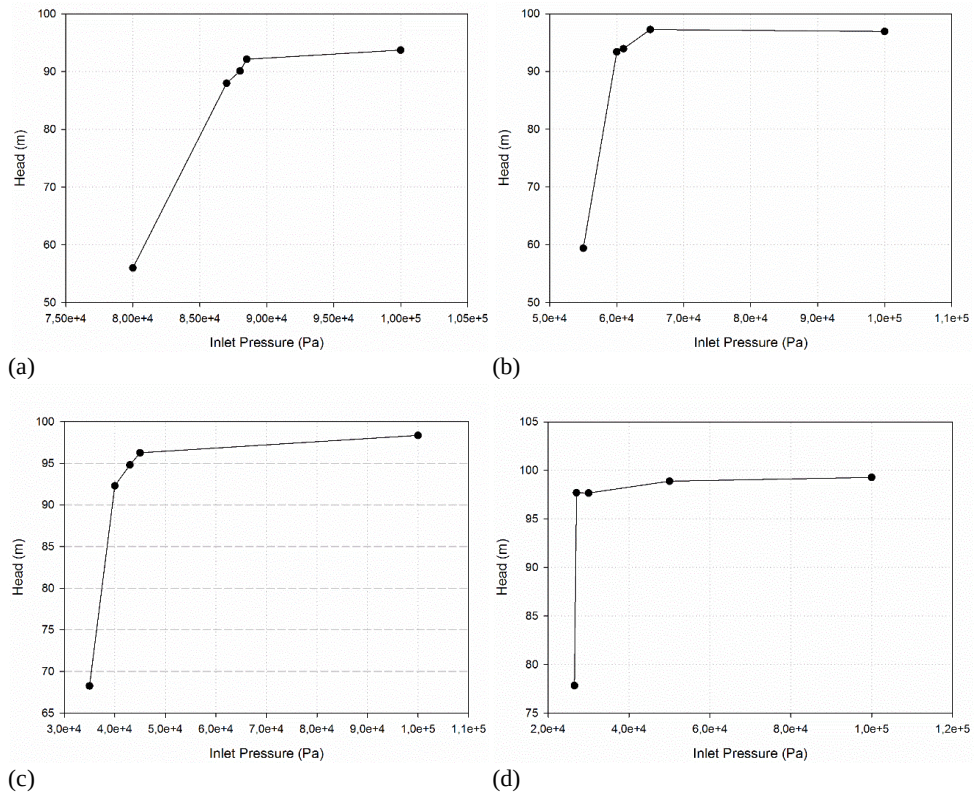

Fig. 12. Cavitation tests of parameterized pump at different flow rates a) 74.8 m3/h, b) 59.9 m3/h, c) 49.7 m3/h, d) 37.1 m3/h.

inlet pressures. The critical inlet pressure values are obtained with the cavitation test and the results are presented in Fig. 12. During the cavitation test procedure, inlet pressure was set at 1 atm and decreased step by step until a 3% head drop is observed.

The critical inlet pressure value (inlet pressure where a 3% head drop is observed) is important because the required net positive suction head ($NPSH_R$) of the pump was calculated with the critical pressure by using the formula below.

$$NPSH_R = \frac{P_c - P_v}{\rho g} \tag{14}$$

According to the calculated $NPSH_R$ values at four different flow rates, the $NPSH_R$ curve of the parameterized pump was obtained, and the results were compared with the experimental results. This comparison can be seen in Fig. 13.

In a similar manner observed in pump characteristic curves, $NPSH_R$ curves were also intersecting at a certain point. Furthermore, the slope of the experimental curve was higher than the parameterized pump's numerical curve. At BEP, the relative error is %14.7 while predicting $NPSH_R$.

To observe the cavitation phenomenon in detail, water vapor volume fractions on the vane surface at four different flow rates are presented in Fig. 14.

It is clearly seen that; the more flow rate increases the more water vapor volume fraction increase on the vane surface. This event is consistent because

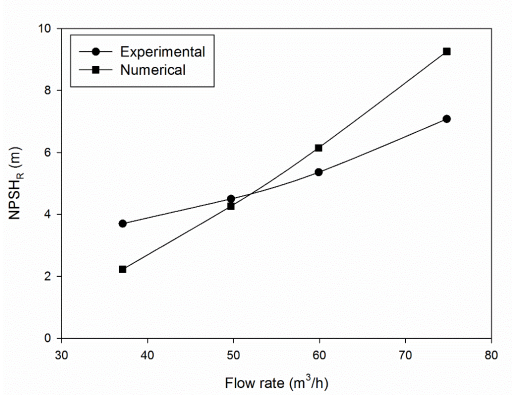

Fig. 13. Comparison of experimental and numerical $NPSH_R$ curves.

according to the numerical cavitation test critical inlet pressure increases with the flow rate which indicates the required load for operating without cavitation increases. This situation explains that the cavitation resistance of the pump decreases with the flow rate. According to the water vapor volume fractions, the pump is exposed to cavitation at the highest flow rate.

Blade loading charts show the pressure distribution along the vane both at suction and pressure sides in a streamwise direction and are useful to observe the cavitation phenomenon. Figure 15 presents the blade loadings on the parameterized pump at different flow rates.

According to the blade loading diagrams at midspan, it is seen that the regions with intense water vapor

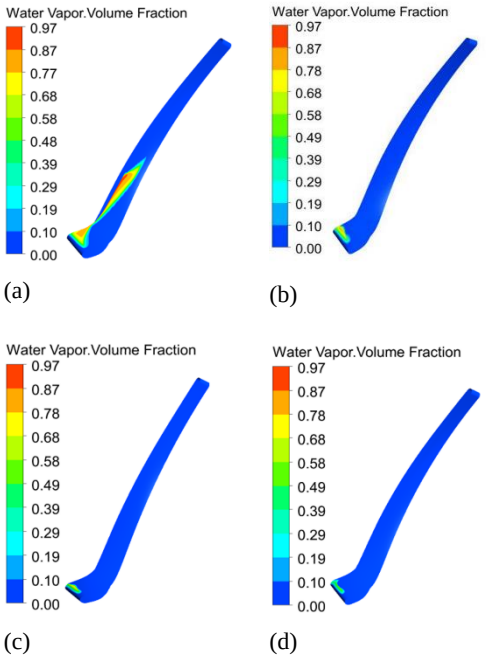

Fig. 14. Water vapor volume fractions on parameterized pump at different flow rates a) 74.8 m3/h, b) 59.9 m3/h, c) 49.7 m3/h, d) 37.1 m3/h.

result in a pressure decrease on the vane. For instance, Fig. 15a clearly shows that a fully developed cavitation is present at the suction side of the vane at 0 and 0.5 streamwise. To sum up, the results of cavitation tests, water vapor volume fractions, and blade loadings are in good agreement with each other.

4. RESULTS AND DISCUSSION

This paper demonstrates how the cavitation behavior of the pump is affected by the variation of inlet vane and wrap angles. For this purpose, a parametric study was carried out and the effect of mentioned angles were investigated both at hub and shroud, separately. The existing pump had different inlet vane and wrap angles at the hub and shroud. Table 3 presents the values of those angles.

4.1 The Influence of Inlet Vane Angle

The study started with an investigation of the inlet vane angle effect on the cavitation behavior of the pump. During this procedure, wrap angles at hub and shroud were set as constants, and investigation of inlet vane angle at hub and shroud were discussed, respectively.

4.1.1. Inlet Vane Angle at Shroud

Firstly, the effect of inlet vane angle at shroud was considered. In addition to the wrap angles at hub and shroud, the inlet vane angle at hub was set as constant. Inlet vane angle at shroud was increased 10° at each step starting from 20° to 50°. Since the inlet vane angle at the shroud was 39°, the design with a 40° inlet vane angle at the shroud was ignored.

A similar approach mentioned in the previous section was implemented. A two-phase 3D CFD study was carried out. Numerical cavitation tests were performed by decreasing the inlet pressure step by step starting from 100,000 Pa. The inlet pressure values where a minimum 3% head drop occurrence was determined and $NPSH_R$ values for each design at four different flow rates were calculated. The results are presented in Fig. 16.

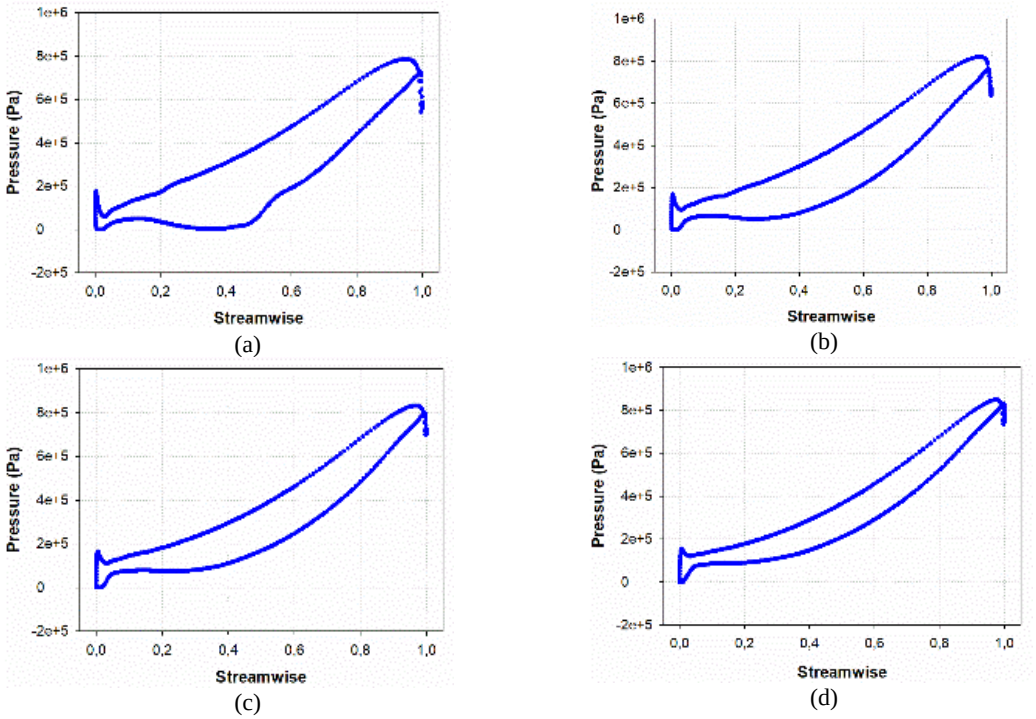

Fig. 15. Blade loadings on parameterized pump at different flow rates a) 74.8 m3/h, b) 59.9 m3/h, c) 49.7 m3/h, d) 37.1 m3/h.

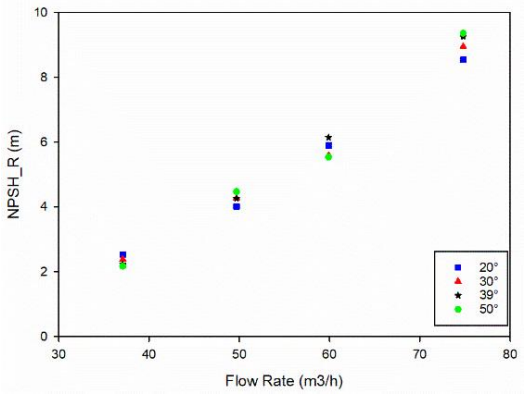

Fig. 16. The influence of inlet vane angle at shroud.

Table 3 Inlet vane and wrap angles of the pump

	Inlet Vane Angle (°)	Wrap Angle (°)
Shroud	39	81
Hub	32	101

According to the table, the variation of inlet vane angle at shroud had a positive influence on BEP (59.9 m3/h). For instance, $NPSH_R$ was decreased to 5.90 at 20°, 5.59 at 30°, and 5.54 at 50° shroud inlet vane angles. However, the increase of inlet vane angle at shroud had resulted in worsening cavitation performance of the pump.

4.1.2. Inlet Vane Angle at Hub

Similarly, a new parametric study was conducted for inlet vane angle at the hub. In this instance, the inlet vane angle at the shroud was constant with wrap angles. Likewise, the inlet vane angle at the hub was increased by 10° at each step. Since the parameterized pump had a 32° inlet vane angle at the hub, it was found unnecessary to carry out simulations for a 30° inlet vane angle at the hub. The $NPSH_R$ values obtained from numerical cavitation tests are demonstrated in Fig. 17.

Results show that $NPSH_R$ decreased with increasing inlet vane angle at the hub. It reached its minimum value at 40° (5.49 m) and increased to 5.79 m at 50° at BEP. Additionally, the decrease in inlet blade angle at the hub resulted in an $NPSH_R$ increase. On the other hand, the increase in inlet vane angle at the hub made the pump operate expose to cavitation. For this reason, $NPSH_R$ values at HF condition were not presented in Fig. 17. At 40° and 50° inlet vane angles at the hub, the head of the pump was 67.81m and 54.50m, respectively, when inlet pressure was 100.000 Pa. This situation shows that the pump operates in cavitating conditions at HF.

4.2 The Influence of Wrap Angle

The next step is to obtain the relationship between wrap angle and cavitation. Similarly, the wrap angle at hub and shroud was examined separately and during this procedure inlet, vane angles at hub and shroud were set as constants.

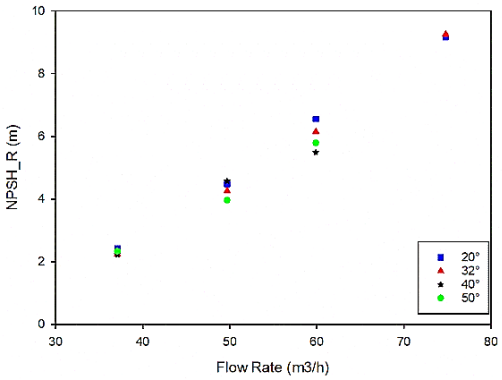

Fig. 17. The influence of inlet vane angle at hub.

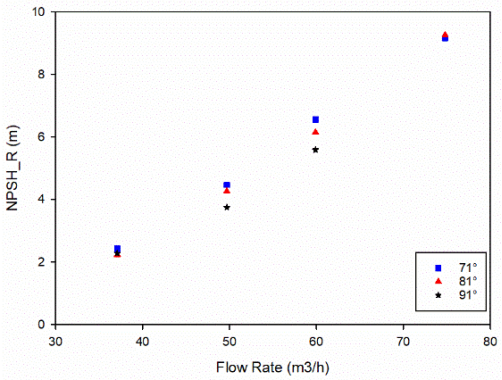

Fig. 18. The influence of wrap angle at shroud.

4.2.1. Wrap Vane Angle at Shroud

In this section, the influence of wrap angle at shroud was examined, and wrap angle at the hub was constant with inlet vane angles. In addition to the 81° wrap angle at the shroud, two more designs were considered with 71° and 91° wrap angles at the shroud. Similarly, numerical cavitation tests were performed with a 3D two-phase study, and the $NPSH_R$ values of each design were calculated for four different operating conditions. The results are shown in Fig. 18.

It is clearly seen that; the cavitation performance of the pump increased with the increasing wrap angle at shroud at BEP because $NPSH_R$ decreased at each step. However, the cavitation behavior of the pump is adversely affected by the wrap angle at shroud increase at HF. Such that, the pump operates under cavitation conditions at a 91° wrap angle at the shroud.

4.2.2. Wrap Angle at Hub

The influence of wrap angle at the hub is discussed for the cavitation behavior of the centrifugal pump. In a similar way, the wrap angle at the shroud was constant with inlet vane angles during this study. After conducting cavitation tests, $NPSH_R$ values of each design were calculated at each operation point and the results are shown in Fig. 19.

As a consequence, it is obvious that both the increase and decrease of wrap angle at the hub had a positive effect on the cavitation performance of the pump.

Even though the cavitation performance increase was higher when the wrap angle at the hub increased to 91° at BEP, the pump was exposed to cavitation at HF. The head of the pump was 54.11 m when the wrap angle at the hub was 91° at HF.

4.3 Design Comparison

According to the numerical cavitation tests performed, the design with a 40° inlet vane angle at the hub resulted in a minimum $NPSH_R$ value (5.49 m) at BEP (Design A). However, this design caused pumps to operate exposed to cavitation at HF. However, the design with a 30° inlet vane angle at shroud (Design B) resulted in cavitation performance improvement both at BEP (5.59 m) and HF (8.95 m). Although the second design does not provide cavitation performance enhancement as much as the first design, a significant performance improvement both at BEP and HF was achieved.

Figures 20 and 21 demonstrated the detailed comparison of the parameterized pump, Design A, and Design B both at BEP and HF. This comparison was presented by means of water vapor volume fractions and blade loadings.

Figure 20 represents the comparison of the three pump models at BEP, respectively. It was seen that water vapor at the suction side of the leading edge is stretching out from hub to shroud. Furthermore, water vapor formation was more annular for Design A.

The situation for operating at HF conditions is presented in Fig. 21 and water vapor occurrence for Design A is extremely high with respect to both parameterized pump and Design B. This situation resulted in low-pressure regions at the suction side of the vane and a pressure increase occurred after 0.6 streamwise.

5. CONCLUSION

This study presents how the cavitation behavior of a centrifugal pump is affected by inlet vane and wrap angle variations. For this purpose, the variation of the inlet vane and wrap angles were investigated both at the hub and shroud. The results of experimental data, numerical simulations, and parameterized pumps were in good agreement with each other. A 3D two-phase CFD study is carried out and the main findings are presented:

Variation of inlet vane angle at shroud resulted in $NPSH_R$ decrease at BEP but the performance increase is only achieved by decreasing the angle at HF. Besides, the decrease in inlet vane angle at the hub helped the pump increase its cavitation performance at BEP. However, these designs are exposed to cavitation at HF. So, decreasing the inlet

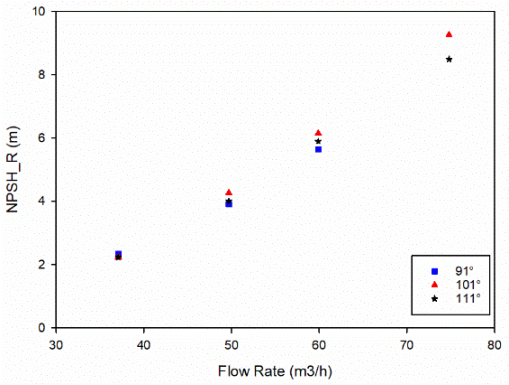

Fig. 19. The influence of wrap angle at hub.

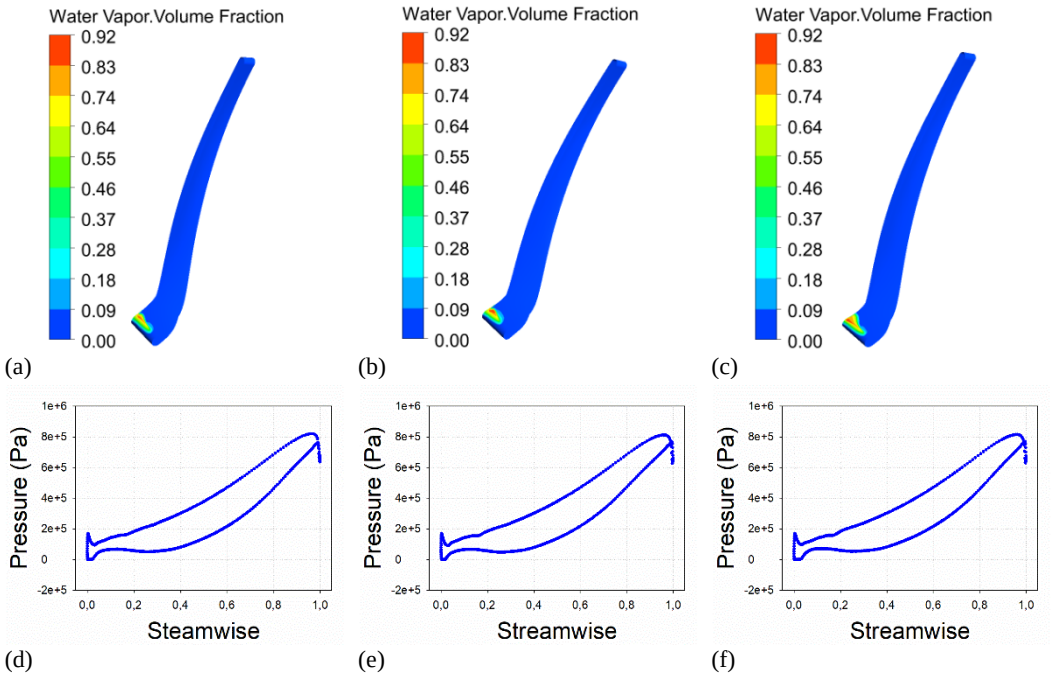

Fig. 20. Water vapor volume fractions for a) parameterized pump, b) Design A, c) Design B, and blade loadings for d) parameterized pump, e) Design A, f) Design B at BEP.

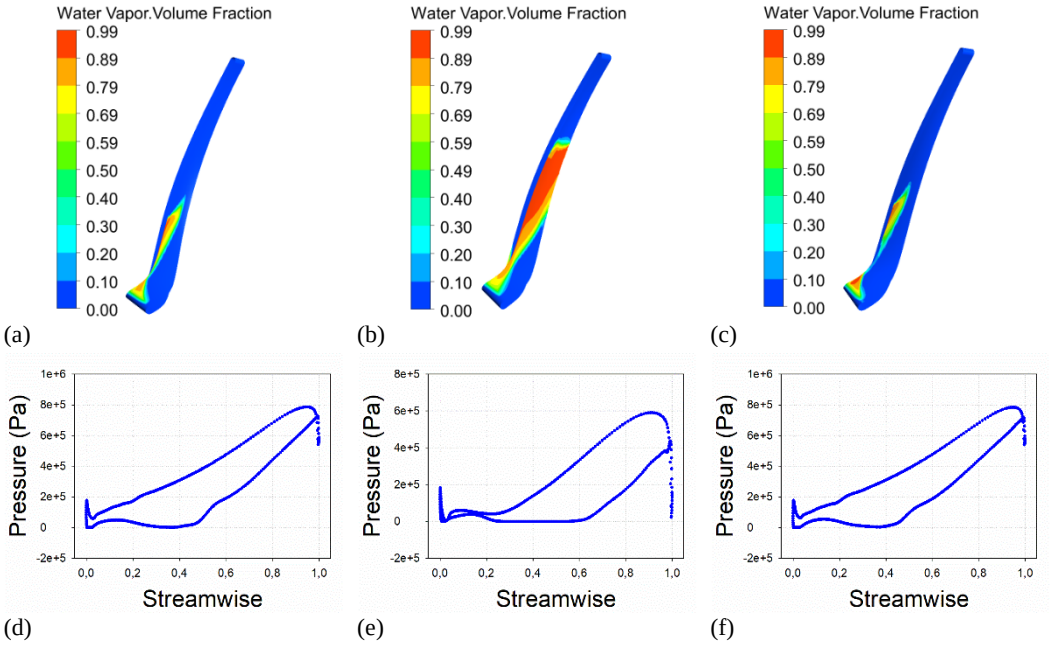

Fig. 21. Water vapor volume fractions for a) parameterized pump, b) Design A, c) Design B and blade loadings for d) parameterized pump, e) Design A, f) Design B at HF.

vane angle at the shroud while keeping the same inlet vane angle at the hub can be suggested for new designs.

The increase in wrap angle at shroud led to cavitation performance enhancement of the pump at BEP but, to operate with cavitation at HF. Both the increase and decrease of the wrap angle at the hub increased the cavitation performance of the pump at BEP. On the other hand, the decrease in $NPSH_R$ is only achieved by increasing the angle at HF. The pump operated under cavitating conditions at HF when the wrap angle at the hub decreased.

Accordingly, increasing the hub wrap angle with a constant shroud wrap angle can be proposed to increase the cavitation performance of the pump.

Design A shows the best cavitation behavior at BEP. Besides, Design B provides a significant improvement of $NPSH_R$ for both BEP and HF so, can be recommended for the existing pump.

ACKNOWLEDGEMENTS

The authors would like to acknowledge Standart Pump Inc. for cooperation.

AVAILABILITY OF DATA AND MATERIALS

Experimental data will not be shared due to the confidential business information of the cooperated company.

AUTHORS' CONTRIBUTIONS

LK and ZY were in charge of the whole trial; AHD carried out the whole numerical simulations and wrote the manuscript. All authors are responsible for conceptualization; read and approved the final manuscript.

FUNDING

Supported by Yildiz Technical University Scientific Research Projects Coordinatorship (Grant No. 2014-06-01-DOP01) and Yildiz Technical University Technopark (Grant No. 14-06-01-DOP01).

COMPETING INTERESTS

The authors declare no competing financial interests.

REFERENCES

Bing, H. and S. Cao (2013) Three-Dimensional Design Method for Mixed-Flow Pump Blades with Controllable Blade Wrap Angle. *Proceedings of the Institution of Mechanical Engineers, Part A: Journal of Power and Energy* 227(5), 567-584.

Bonaiuti, D., M. Zangeneh, R. Aartojarvi and J. Eriksson (2010) Parametric Design of a Waterjet Pump by Means of Inverse Design, CFD Calculations and Experimental Analyses. *Journal of Fluids Engineering* 132(3), 031104.

Brennen, C. E. (1995). *Cavitation and Bubble Dynamics*. Oxford University Press, New York.

Christopher, S. and S. Kumaraswamy (2013) Identification of Critical Net Positive Suction Head from Noise and Vibration in a Radial Flow Pump for Different Leading Edge Profiles of the Vane. *Journal of Fluids Engineering* 135(12), 121301.

Coutier-Delgosha, O., R. Fortes-Patella, J. L.

Reboud, M. Hofmann and B. Stoffel (2003). Experimental and Numerical Studies in a Centrifugal Pump with Two-Dimensional Curved Blades in Cavitating Condition. *Journal of Fluids Engineering* 125(6), 970-978.

Dönmez, A. H., Z. Yumurtacı and L. Kavurmacıoğlu (2019). The Effect of Inlet Blade Angle Variation on Cavitation Performance of a Centrifugal Pump: A Parametric Study. *Journal of Fluids Engineering* 141(2), 021101.

Friedrichs, J. and G. Kosyna (2002). Rotating cavitation in a centrifugal pump impeller of low specific speed. *Journal of Fluids Engineering* 124(2), 356-362.

Gaetani, P., A. Boccazzi and R. Sala (2012) Low Field in the Vaned Diffuser of a Centrifugal Pump at Different Vane Setting Angles. *Journal of Fluids Engineering* 134(3), 031101.

Kang, C., N. Mao, W. Zhang and Y. Gu (2017). The Influence of Blade Configuration on Cavitation Performance of a Condensate Pump. *Annals of Nuclear Energy* 110, 789–797.

Li, X., S. Yuan, Z. Pan, J. Yuan and Y. Fu (2013). Numerical Simulation of Leading Edge Cavitation within the Whole Flow Passage of a Centrifugal Pump. *Science China Technological Sciences* 56(9), 2156-2162.

Liu, H. L., D. X. Liu, W. Yong, X. F. Wu, W. A. N. G. Jian and D. U. Hui (2013). Experimental Investigation and Numerical Analysis of Unsteady Attached Sheet Cavitating Flows in a Centrifugal Pump. *Journal of Hydrodynamics, Ser. B* 25(3), 370-378.

Lu, J., S. Yuan, P. Siva, J. Yuan, X. Ren and B. Zhou (2017). The Characteristics Investigation under the Unsteady Cavitation Condition in a Centrifugal Pump. *Journal of Mechanical Science and Technology* 31(3), 1213-1222.

Luo, X., W. Wei, B. Ji, Z. Pan, W. Zhou and H. Xu (2013). Comparison of Cavitation Prediction for a Centrifugal Pump with or Without Volute Casing. *Journal of Mechanical Science and Technology* 27(6), 1643-1648.

Luo, X., Y. Zhang, J. Peng, H. Xu and W. Yu (2008.). Impeller Inlet Geometry Effect on Performance Improvement for Centrifugal Pumps. *Journal of Mechanical Science and Technology* 22(10), 1971–1976.

Menter, F. R. (1994). Two-Equation Eddy-Viscosity Turbulence Models for Engineering Applications. *AIAA Journal* 32(8), 1598-1605.

Mousmoulis, G., N. Karlsen-Davies, G. Aggidis, I. Anagnostopoulos and D. Papantonis (2019). Experimental Analysis of Cavitation in a Centrifugal Pump Using Acoustic Emission, Vibration Measurements and Flow Visualization. *European Journal of Mechanics - B/Fluids* 75, 300-311.

Pei, J., T. Yin, S. Yuan, W. Wang and J. Wang (2017). Cavitation Optimization for a Centrifugal Pump Impeller by Using Orthogonal Design of Experiment. *Chinese Journal of Mechanical Engineering* 30(1), 103-109.

Shao, C., C. Li and J. Zhou (2018). Experimental Investigation of Flow Patterns and External Performance of a Centrifugal Pump That Transports Gas-Liquid Two-Phase Mixtures. *International Journal of Heat and Fluid Flow* 71, 460-469.

Shim, H. S., K. Y. Kim and Y. S. Choi (2018). Three-Objective Optimization of a Centrifugal Pump to Reduce Flow Recirculation and Cavitation. *Journal of Fluids Engineering* 140(9), 091202.

Tan, L., Zhu, B., Cao, S., Bing, H., and Wang, Y. (2014a). Influence of Blade Wrap Angle on Centrifugal Pump Performance by Numerical and Experimental Study. *Chinese Journal of Mechanical Engineering* 27(1), 171-177.

Tan, L., Zhu, B. S., Cao, S. L., Wang, Y. C., and Wang, B. B. (2014b). Numerical Simulation of Unsteady Cavitation Flow in a Centrifugal Pump at Off-Design Conditions. *Proceedings of the Institution of Mechanical Engineers, Part C: Journal of Mechanical Engineering Science* 228(11), 1994-2006.

Valentini, D., G. Pace, A. Pasini, L. Torre, R. Hadavandi and L. d'Agostino (2017). Fluid-Induced Rotordynamic Forces on a Whirling Centrifugal Pump. *European Journal of Mechanics - B/Fluids* 61, 336-345.

Vujanic, V. and B. Velensek (1994). Influence of Cavitation on Blade Characteristics. *Experiments in Fluids* 17(6), 441–445.

Weidong, C., L. Yue and Z. Xiaodi (2009). Study on Performance of Low Specific Speed Sewage Pump with Different Vane Wrap Angles. *Irrigation and Drainage* 6, 004.

Xu, Y., L. Tan, S. Cao and W. Qu (2016). Multiparameter and Multiobjective Optimization Design of Centrifugal Pump Based on Orthogonal Method. *Proceedings of the Institution of Mechanical Engineers, Part C: Journal of Mechanical Engineering Science* 231(14), 2569–2579.

Ye, Y., X. Zhu, F. Lai and G. Li (2017). Application of the Semi-Analytical Cavitation Model to Flows in a Centrifugal Pump. *International Communications in Heat and Mass Transfer* 86, 92–100.

Yokoyama, S. (1960). Effect of the Tip Shape at Entrance of the Impeller Vane of the Centrifugal Pump on Cavitation. *Bulletin of Japan Society of Mechanical Engineers* 3(11), 326–332.

Zhang, N., X. Liu, B. Gao, X. Wang and B. Xia (2019). Effects of Modifying the Blade Trailing Edge Profile on Unsteady Pressure Pulsations and Flow Structures in a Centrifugal Pump. *International Journal of Heat and Fluid Flow* 75, 227-238.